[illegible] FILE COPY

(2)

REPORT DOCUMENTATION PAGE

Form Approved
OMB No. 0704-0188

Public reporting burden for this collection of information is estimated to average 1 hour per response, including the time for reviewing instructions, searching existing data sources, gathering and maintaining the data needed, and completing and reviewing the collection of information. Send comments regarding this burden estimate or any other aspect of this collection of information, including suggestions for reducing this burden, to Washington Headquarters Services, Directorate for Information Operations and Reports, 1215 Jefferson Davis Highway, Suite 1204, Arlington, VA 22202-4302, and to the Office of Management and Budget, Paperwork Reduction Project (0704-0188), Washington, DC 20503.

AD-A232 036

1. AGENCY USE ONLY (Leave blank)

2. REPORT DATE: Oct. 30, 1990

3. REPORT TYPE AND DATES COVERED: Final Report 9/1/87 - 8/31/90

4. TITLE AND SUBTITLE: Wavelength Independent Optical Lithography and Microscopy

5. FUNDING NUMBERS: G AFOSR-87-0381

6. AUTHOR(S): Michael Isaacson

7. PERFORMING ORGANIZATION NAME(S) AND ADDRESS(ES):
Cornell University
College of Engineering
School of Applied and Engineering Physics
Clark Hall, Ithaca, New York 14853

8. PERFORMING ORGANIZATION REPORT NUMBER: AFOSR-TR- 91 0022

9. SPONSORING/MONITORING AGENCY NAME(S) AND ADDRESS(ES):
Air Force Office of Scientific Research
Electronic and Materials Science
AFOSR/NE (Bldg. 410)
Bolling AFB
Washington, DC 20332-6448

10. SPONSORING/MONITORING AGENCY REPORT NUMBER: 2306/B1

DTIC ELECTE FEB 19 1991 S B D

11. SUPPLEMENTARY NOTES

12a. DISTRIBUTION/AVAILABILITY STATEMENT:
Approved for public release;
distribution unlimited.

12b. DISTRIBUTION CODE

13. ABSTRACT (Maximum 200 words)

During this past contract period we have successfully established the field of near-field optics and subwavelength light beam technology. We have experimentally verified some of the physical parameters upon which the collimation of light in the near-field depends and have demonstrated that collimation better than one tenth the wavelength can be achieved in both transmission imaging and reflection imaging and that lithographic replication at one fifth the wavelength is attainable. In addition, we have also demonstrated that darkline defects in GRIN-SCH-SQW diode lasers can be directly observed at high spatial resolution using the methods of lenseless near-field imaging.

14. SUBJECT TERMS: near-field optics, subwavelength light beam technology, optical lithography

15. NUMBER OF PAGES: 47

16. PRICE CODE

17. SECURITY CLASSIFICATION OF REPORT	18. SECURITY CLASSIFICATION OF THIS PAGE	19. SECURITY CLASSIFICATION OF ABSTRACT	20. LIMITATION OF ABSTRACT
Unclassified	Unclassified	Unclassified	UL

FINAL REPORT
AFOSR - 87 - 0381

"WAVELENGTH INDEPENDENT OPTICAL LITHOGRAPHY AND MICROSCOPY"

PROGRESS BETWEEN 9/1/87 - 8/31/90

PROFESSOR MICHAEL ISAACSON
CORNELL UNIVERSITY
SCHOOL OF APPLIED AND ENGINEERING PHYSICS
CLARK HALL, ROOM 201
ITHACA, NEW YORK 14853

91 2 11 197

TABLE OF CONTENTS

I.	ABSTRACT	1
II.	PROGRESS REPORT (AFOSR 87-0381)	2
	A. BASIS OF NEAR-FIELD OPTICAL TECHNOLOGY	2
	B. CHARACTERISTICS OF NEAR-FIELD OPTICAL IMAGING	3
	C. NEAR-FIELD OPTICAL LITHOGRAPHY	7
	D. DIRECT NEAR-FIELD DIAGNOSTICS OF LASER EMISSION PATTERNS	8
	E. REFERENCES CITED	9
III.	APPENDICES	40
	A. INVITED TALKS PRESENTING RESEARCH PERFORMED UNDER CONTRACT AFOSR 87-0381	41
	B. PAPERS PUBLISHED UNDER THIS CONTRACT	43
	C. INVITED MANUSCRIPTS IN PREPARATION RELATING TO PRESENT CONTRACT RESEARCH	44
	D. STUDENTS PERFORMING RESEARCH ON NEAR-FIELD IMAGING/FABRICATION	45

Accession For		
NTIS GRA&I		☑
DTIC TAB		☐
Unannounced		☐
Justification		
By		
Distribution/		
Availability Codes		
Dist	Avail and/or Special	
A-1		

I. ABSTRACT

During this past contract period we have successfully established the field of near-field optics and subwavelength light beam technology. We have experimentally verified some of the physical parameters upon which the collimation of light in the near-field depends and have demonstrated that collimation better than one tenth the wavelength can be achieved in both transmission imaging and reflection imaging and that lithographic replication at one fifth the wavelength is attainable. In addition, we have also demonstrated that darkline defects in GRIN-SCH-SQW diode lasers can be directly observed at high spatial resolution using the methods of lenseless near-field imaging.

II. PROGRESS REPORT

Over the last three years, under AFOSR Contract #87-0381 we have developed a new field of optics based upon the collimation of near-field radiation. Near-field optics allows spatial resolution far exceeding the conventional far-field diffraction limit and allows for the production of light beams of diameter more than an order of magnitude smaller than their wavelength. Thus, technology based upon near-field optics offers the promise of *sensitive non-destructive* surface characterization of materials at super spatial resolution and the ability to fabricate structures on the 10's of nm scale using these near-field collimated optical beams.

As a direct result of the AFOSR sponsored research on near-field optics at Cornell, the field of near-field imaging has blossomed. In Figure 1 we show how the number of groups directing research in this area has expanded during the last half decade. Almost half of all the groups doing research in near-field optical technology have received aid from the Cornell group either by visits to our laboratory or invited visits by the PI to their laboratories (see list of invited presentations in Appendix A).

During this present contract period we have successfully completed construction of a scanning near-field optical microscope that operates in reflection and transmission using visible and near infrared wavelengths. We have developed a technology for guiding light beams to form 50nm diameter probes and have begun preliminary measurements and calculations to characterize this technology. We have shown that structures of the order of 100nm can be successfully replicated using near-field optical technology. In addition, we have demonstrated that the near-field technique should be an extremely sensitive method of characterizing metallic, dielectric and transparent surfaces and that direct near-field imaging can be used as a diagnostic tool for investigating the modal field patterns of semiconductor laser diodes at spatial resolutions approaching one tenth the wavelength of the emitted radiation. In this section we will describe briefly some of the advances that we have made during the three years of the present contract.

II. A. Basis of Near-Field Optical Technology

The underlying concept of near-field optical technology is illustrated in Figure 2. Incident radiation is incident upon an opaque screen containing an aperture of subwavelength diameter. The radiation emanating through the aperture is first collimated to the aperture size. In the exit region in the proximity of the aperture, the radiation still is collimated to the aperture size rather than determined by the wavelength -- the near-field regime. Eventually, far from the screen (in terms of the wavelength), the diverging radiation pattern is that of far-field diffraction and is no longer a geometrical image of the aperture but rather related to the Fourier transform of the aperture. Thus, putting a sample in this "near-field" allows us to illuminate a region whose size is significantly smaller than

the illuminating wavelength.

This collimation effect has been calculated in detail for an infinitely long slit in a thick screen (Betzig, et al. 1986) and a calculation of the power transmitted through a circular aperture in a thin screen is shown in Figure 3. As it turns out, the region near the aperture where the light beam is collimated extends to about the aperture diameter/π. In fact, the full width at half maximum of the transmitted intensity only increases by about 10% at that distance (Harootunian, 1987). In the region of visible light wavelengths there is of course no such thing as a perfectly conducting screen and so the skin depth of the screen material will also enter into the determination of the degree of collimation expected.

It should also be noted that this collimation effect can be used in reverse. If we look again at Figure 2, we see that if the sample surface is "self-luminous" then only light emitted from a region of the surface about the size of the aperture will be collected by the aperture and can be detected on the opposite side. By raster-scanning the aperture relative to the surface and using the detected light to intensity modulate a display, we thus obtain a near-field scanning optical microscope (NSOM) image. A schematic illustration of the modes of near-field imaging that we have successfully implemented under this contract is shown in Figure 4 using an aperture at the end of a metallized glass pipette as the "optical receiver". Note that Figure 4A could also represent that of near-field imaging of a "self-luminous" object if the sample surface were the light source. The important point is that only the near-field region is imaged at high spatial resolution, regions outside the near-field just contribute a low contrast, low resolution background "fog". We have performed several fundamental experiments illucidating the contributions to this near-field collimation and which illustrate certain features of near-field radiation. These are described in section II.B.

II. B. Characteristics of Near-Field Optical Imaging

During this contract period, we have developed the metallized glass pipette as the "aperture on a pinnacle" needed for successful near-field surface imaging. A schematic of this "aperture" is shown in Figure 5. The pipettes are drawn using pipette pullers of the type used for fabricating patch clamp pipettes for cell biology experiments (e.g., Brown and Flaming, 1986). We have spent some time developing the technology for controlling the diameter and shape of these capillary tubes (pipettes) in order to understand the light transmitting properties of these structures. The outer portion of these pipettes are metallized for light guiding properties as well as to prevent extraneous light from being transmitted through the walls of the pipette. The taper of the tip of the pipette is important since in the "aperture" region the light wave is evanescent (the light guide is below the cut-off frequency). In this evanescent region, the light beam intensity decays exponentially,

thus an engineering balance between the taper angle, θ, the thickness of the metal overcoating and the outer diameter of the pipette is crucial. Changes in tip end geometry can change the transmitted intensity by an order of magnitude.

Since the optical properties of these light guides are crucial for designing microscopy/inspection experiments (applications) and in looking at nanometer scale lithography considerations, we have initiated experiments to evaluate the transmission characteristics of these pipette apertures. In Figure 6 we show the result of some preliminary measurements of the transmission coefficient through such metallized pipette apertures. Note that although small thickness metal overlayers (i.e., small t) give better transmission, they also result in less attenuation of light incident on the metal and thus the contrast (light through aperture/light through metal) is reduced. We need to further investigate radiation transmission through these structures since most theories consider only the case of perfectly conducting screens.

Examples of these pipettes and metallized pipettes are shown in Figures 7-9. In Figure 7 we just show an array of these pipettes after the metallization step. All of these pipettes are inspected in an SEM to completely characterize the "optical tip" geometry and to investigate the structure and texture of the metal coating which is critical for proper light guiding. Figure 8 shows SEM micrographs of the drawn glass pipettes showing that 50nm diameter holes can be produced and that ends as small as 25nm can be fabricated. In Figure 9a we show similar pipettes that have been metallized with chromium (top) and aluminum (bottom) and fabricated from borosilicate glass. Aluminum is the preferred material using visible radiation because of its high extinction coefficient although its large grain size sometimes precludes being able to position the pipette aperture in the near-field due to nucleation growth at the pipette edges. In Figure 9b we show pipettes which are the result of fabricating pipette apertures from aluminosilicate glass rather than borosilicate glass used on the previous figure. The advantage of using aluminosilicate glass is that because of its different melting point, the end is slightly fire-polished during the pulling process resulting in rounded edges on the tip (more closely approaching the aperture on a pinnacle). The smoother surface also allows for more uniform film growth as can be seen by comparing Figure 9b with Figure 9a. Another advantage of this glass is that one obtains smaller OD/ID ratios resulting in a more single mode propogation characteristic up along the pipette.

During this last contract period we have completed the construction of the scanning near-field optical system designed earlier. It is shown in Figure 10 and the design has been described in detail before (e.g., Betzig, et al. 1988, Betzig, 1988). Significant improvements have been made in pipette technology, electronics and detection sensitivity. The main point to note is that when we started construction on this instrument, we chose to use a piezo-driven scanning stage rather than scanning the pipette aperture itself in order to obtain near-field images. This has somewhat reduced the flexibility in using the instrument for different applications

since the mass of the sample and sample holder becomes critical from the point of view of scanning mechanical resonances and hysterisis. This will be alleviated in the next instrument. The pipette mounted in a piezo-electric tube and aluminum holder is shown in Figure 11. The piezo tube provides the fine positioning perpendicular to the sample and can be used in a capacitance or tunneling feedback loop to control "optical tip" height above the sample. Another view of the "tip" over a sample is shown in Figure 24.

In order to characterize the near-field radiation for imaging and fabrication purposes, we fabricated (at the Cornell National Nanofabrication Facility) a series of metal structures on thin Si_3N_4 membranes and bulk Si wafers. The membranes allowed us to obtain images in transmission and reflection. Although transmission imaging is only of use for transparent samples it is conceptually easier to understand (and calculate). Our aim was to see how the near-field collimation depended on various physical parameters and to compare (whenever possible) near-field images with conventional optical images or SEM images.

In Figure 12A we show an SEM micrograph of 250nm wide aluminum bars 25nm thick arranged in a grating fashion. In Figure 12B is shown the corresponding near-field transmission images obtained with a 100nm diameter pipette and a broadband illumination source using a 450nm cut-off filter (i.e., $\lambda \geq 450$nm). Note that there appears to be huge intensity peaks (white spots) near the ends of the aluminum bars (dark) which is due to the "amplification" of the near-field radiation at the edge of metal structures. This effect has been qualitatively explained by the electromagnetic calculations of Marx and Teague at NIST who were looking at the possibilities of using these high intensity peaks at metal edges to develop a more reliable line width metrology tool (Marx and Teague, 1987).

In Figure 13 we show one of the early images obtained with our near-field optical microscope. Note that a larger diameter pipette collector results in poorer lateral resolution in the near-field image than that obtained with a smaller aperture. This is as expected based upon the nature of the near-field collimation. In Figure 14 we show a comparison of a conventional near-field optical image of a transparent thin section of human skeletal muscle. The images were both obtained using white light illumination with a 450nm cut off filter to eliminate the UV contribution to the image. The point to note here is that the near-field image only reveals the surface details and not information from the entire section thickness; most of that is "out of focus" because it is not in the near-field.

Thus, we have shown the aperture collector dependent properties of near-field imaging and that only surface structure is probed. Next we show in Figure 15 essentially a "through focus" series of scanning pipette images where the distance between the optical receiver tip and the sample is varied. These images were obtained with a 60nm diameter aperture and it is clear that only in the "near-field" image is 50nm lateral resolution seen. Thus, this series indicates the collimated

nature of near-field radiation.

In addition, we have also investigated the effect of coherence and polarization of the illuminating source on the resulting near-field imaging. Our initial experiments indicate that there can be significant polarization effects. This can be seen in Figure 16 in transmission and in Figure 17 in reflection. In Figure 16 the axes of the polarization induced pattern is always aligned in the direction of the crystal axes of the silicon substrate used to form the Si_3N_4 membranes. Thus, it appears that the near-field technique may be capable of polarization induced contrast. Calculations and measurements by Fischer et al. (1987) for a simple aperture scanning over an aperture in the near-field indicate that such polarization effects may be present. In Figure 17b we show polarization dependance of collected reflected light from aluminum surfaces using broadband white light illumination. Here the geometry is that shown in Figure 4b. We hope to be able to further investigate this phenomenon in order to determine its utility in characterizing strain in thin film materials or surfaces. The distinct change in intensity vs. distance in the near field region also affords us the possibility of using this change as a feedback mechanism of the aperture height above the sample surface.

In examining the spatial resolution achievable in near-field imaging, we show in Figure 18-19 examples of lateral resolution approaching 60nm using visible light. In Figure 18 is shown a near-field image of an array of 60nm diameter, 25nm thick Al posts on a Si_3N_4 membrane. And in Figure 19 we show a comparison of the near-field reflection and transmission images of the same set of Al bars. Lower lateral resolution complementary images in transmission and reflection are shown in Figure 20. The resolution is consistent with the aperture size and aperture to sample separation. Although there have been previous reports of reflection near-field imaging using a different method (Fischer et al., 1988), these tests are the <u>first definitive measurements</u> of the lateral resolution of the method.

Finally, the potential surface sensitivity of near-field imaging is illustrated in Figure 21A where we show the reflection image of aluminum "quantum" dots on a bulk silicon substrate taken with a pipette 10nm from the surface using white light illumination. The upper figure is the near-field optical image taken at the same magnification as the SEM micrograph of a similar field of dots on the same sample. Note the very high contrast of the "swirls" around the small 100nm dots in the near-field image. This appears to be about 20Å thick surface scum left over as a result of the incomplete removal of the resist during the lift off process used to fabricate the Al dots. It is barely visible in the SEM picture even though the image was obtained using the highest contrast. Thus, these initial images indicate the potential of near-field imaging for detecting nm thickness material on surfaces. Ultimately we hope to be able to couple the imaging with spectroscopic determination of the material composition.

In Figure 21B, we show lower magnification reflection images of the same sample. The images have been obtained for different distances of the pipette aperture from the sample. In the far-field image (pipette positioned about 1.6 wavelengths away from the sample), we effectively see bright but broadened reflected intensity dots that appear to come from the aluminum posts. The image drastically changes upon moving the pipette into the near-field (pipette positioned about one tenth a wavelength away from the sample). The character of the near-field image is strikingly different from the far-field one.

II. C. Near-Field Optical Lithography

Another potential utilization of the near-field collimation effect is in the area of nanometer scale fabrication. Current optical printing techniques are pushing towards the 300nm scale using very deep UV radiation. There exists the possibility of far exceeding that limit while using softer UV radiation by exploiting near-field technology. During this present contract period we chose to investigate near-field contact printing to see what difficulties lay ahead, to estimate the lateral resolution of the method and determine whether sufficient near-field transmission through an opaque stencil mask would enable exposure of underlying resist.

The key to this method is to utilize a very thin resist imaging layer, since the near-field radiation will only be collimated for a distance of the order of the mask feature sizes. Our aim was to replicate 100nm structures using a standard Hg-Xe lamp with a 450nm cut-off filter. In order to achieve this goal we utilized 60nm thick spun-on Shipley 1400 photoresist as our imaging layer.

In Figure 22 we show an SEM micrograph of a pattern exposed directly in the 60nm resist by contact printing a pattern in a metallized Si_3N_4 membrane stencil mask. The stencil mask was fabricated using a process technology developed at Cornell (Muray, et al., 1983). One can see that this simple process demonstrates 120nm line replication on a 250nm pitch.

By itself, the patterned thin film resist is not of much practical use since real structures that one must pattern are not necessarily smooth surfaces. Thus, we explored the use of a trilevel resist system which could be patterned in the near-field (i.e., using the same 60nm imaging layer of Shipley 1400), but would still allow us to cover rough surfaces and to be thick enough to act as an etch mask.

A polyester polymer, Futurex 1500d was chosen as the planarizing layer because of its fast etch rate in an O_2 plasma. Futurex IC1-200 spin-on-glass was used as the intermediate layer because it has good etch resistance to O_2 plasma. The trilevel process is shown in Figure 23 along with the SEM micrographs of the results. The exposure was done through a membrane stencil mask as before and as

can be seen, 120nm lines have been replicated indicating the potential of near-field lithography.

II. D. Direct Near-Field Diagnostics of Laser Emission Patterns

One of the advantages of near-field collimation used for imaging is that the spatial resolution attainable is to first order independent of the wavelength of the imaging radiation. A potentially important use of this method could be in the diagnostics of the near-field emission patterns of quantum well hetrostructure semiconductor lasers. The conventional method of imaging of these patterns is by imaging the emitted light through a lens positioned such that the laser face is imaged on a CCD array (Peled, 1980). The problem with this method is that the lateral resolution is far-field diffraction limited (to at best $\lambda/2$) which restricts its usefulness as a diagnostic tool when developing new laser concepts since defects in the material and the mode structure can in fact result in light modulation on a much smaller scale.

Lateral resolution an order of magnitude better than that attained with conventional techniques affords us the possibility of more accurately assessing the effect of growth parameters on the emitted light output distribution. The direct near-field imaging technique (using a scanned pipette aperture) is ideally suited for such diagnostics. We have received $Al_xGa_{1-x}As$ graded-index separate confinement hetrostructure single quantum well lasers (GRIN-SCH-SQW) from Dr. Chet Balestra of McDonnell-Douglas Electronic Systems Company in order to investigate this concept. The lasers had a linearly compositionally graded index of about 450nm on either side of a 10nm quantum well as described by Waters (Waters et al., 1988). They were mounted in the near-field microscope assembly (Figure 10) vertically with respect to the optical pipette tip to be used as the receiver (Figure 24). The same photomultiplier detection system was used as for the experiments using visible light even though the quantum efficiency of the tube was two orders of magnitude smaller at the IR emission wavelength of 860nm of the laser than in the previous experiments using visible light.

In Figure 25 we show the results of the modal field pattern from one such laser that was thought to have had fabrication induced material strain. The image in which the optical tip was a distance of 2/3 wavelengths away from the laser facet is similar in resolution to the conventional "near-field" images obtained using lenses focused on the laser face. Clearly the near-field scanning optical microscopy (NSOM) technique is capable of displaying higher resolution structure than the conventional method. One point to note in the near-field image obtained at $\lambda/100$ distance from the laser facet is the possible evidence that we can observe dark line defects (Waters and Bertaska, 1988) directly. This can perhaps be better seen in the series of intensity line scans across the laser facet in the near-field (see Figure 26)

where we can see the dip in intensity in the vicinity of the "rabbit ear" lobes. An example of a more uniform pattern from a "good" laser is shown in Figure 27. Thus, near-field imaging using scanned optical tips looks potentially like an extremely useful diagnostic tool for materials and device development of QW type lasers.

In summary, experiments under the present contract during the last three years have demonstrated a practical instrument for investigating near-field optics and have shown the potential of near-field light beam technology for fabrication and diagnostic/inspection of optical and optoelectronic materials.

II. E. References Cited

Betzig, E., A. Harootunian, A. Lewis and M. Isaacson. (1986) Applied Optics 25, 1890-1900.

Betzig, E., M. Isaacson, H. Barshatzky, A. Lewis and K. Lin (1988) Proc. SPIE Vol. 897, 91-99

Betzig, E. (1988) Ph.D. Dissertation, Cornell University

Brown, K.T. and D.G. Flaming (1986) "Advanced Micropipette Techniques for Cell Physiology (John Wiley and Sons, New York).

Fischer, U-Ch., U. Durig and D.W. Pohl (1987) Scanning Microscopy Suppl. 1, 47-52.

Fischer, U-Ch., U. Durig and D.W. Pohl (1988) Appl. Phys. Lett. 52(4), 249-251.

Harootunian, A. (1987) Ph.D. Dissertation, Cornell University

Marx, E. and E.C. Teague (1987) Appl. Phys. Lett. 51(25), 2073-2075.

Muray, A., M. Isaacson, I. Adesida and B. Whitehead (1983) J. Vac. Sci. Technol. B1(4), 1091-1096.

Peled, S. (1980) Applied Optics 19(2), 324-328.

Roberts, A. (1987) J. Opt. Soc. Amer. A4(10), 1970-1983.

Waters, R.G. and R.K. Bertaska (1988) Appl. Phys. Lett. 52(16), 1347-1348.

Waters, R.G. and D.S. Hill and S.L. Yellen (1988) Appl. Phys. Lett. 52(24), 2017-2018.

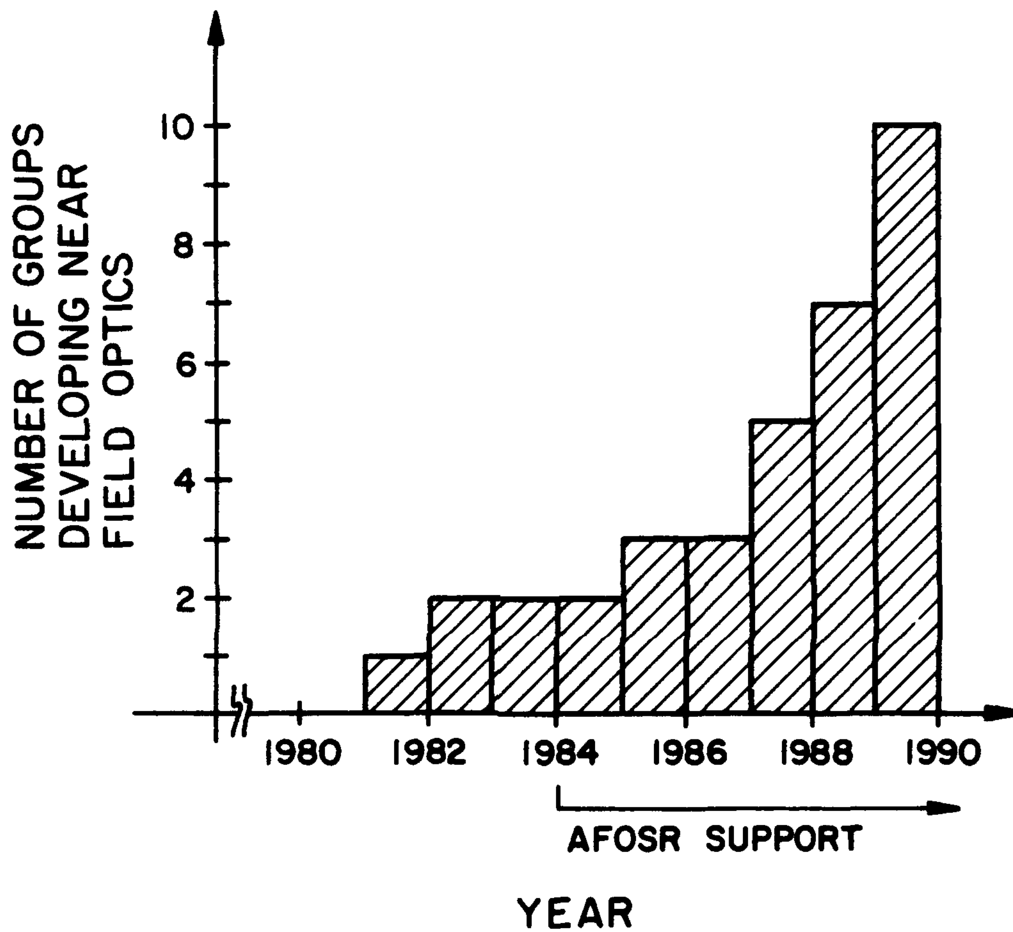

Figure 1: Histogram of the number of groups performing research in near-field optical technology as a function of year. Since the beginning of AFOSR support, the number has increased five fold and it is anticipated that the current number will double by 1992.

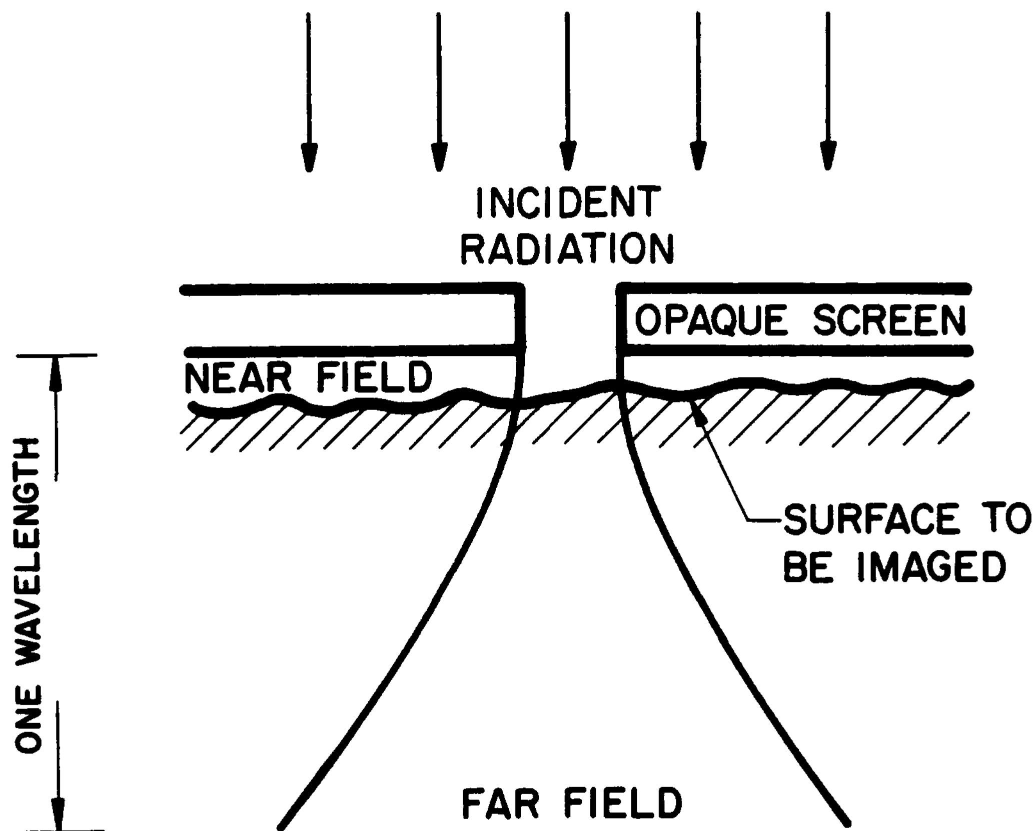

Figure 2: Schematic representation showing the collimation of radiation emanating from a subwavelength aperture. Alternatively, this schematic can be looked upon as showing the radiation emanating from a luminous subwavelength object.

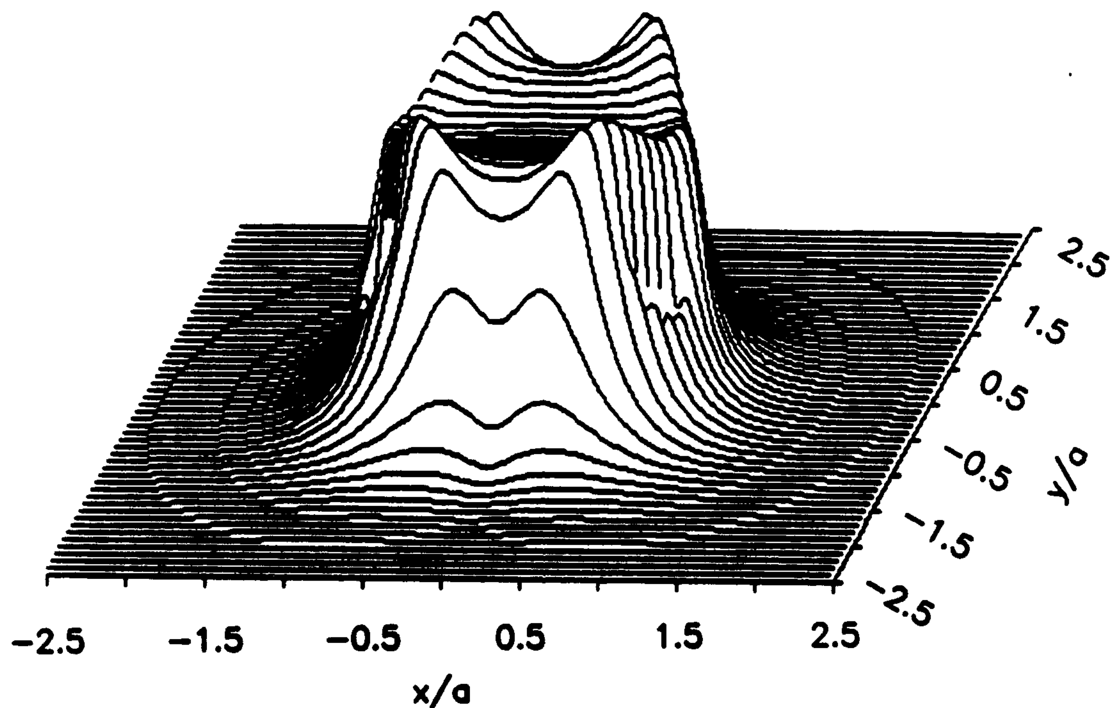

Figure 3: Calculation of the intensity (the Poynting vector, S) emanating from an aperture in a perfectly conducting thin screen. The aperture radius, a, is 1/50th of the illuminating radiation wavelength, λ, and the lateral coordinates (x,y) are in units of the aperture radius. The intensity has been calculated at a distance of a/10 from the screen. The full width at half maximum of the intensity distribution increases by only about 10% at distances up to the aperture radius from the screen (from Harootunian, 1987).

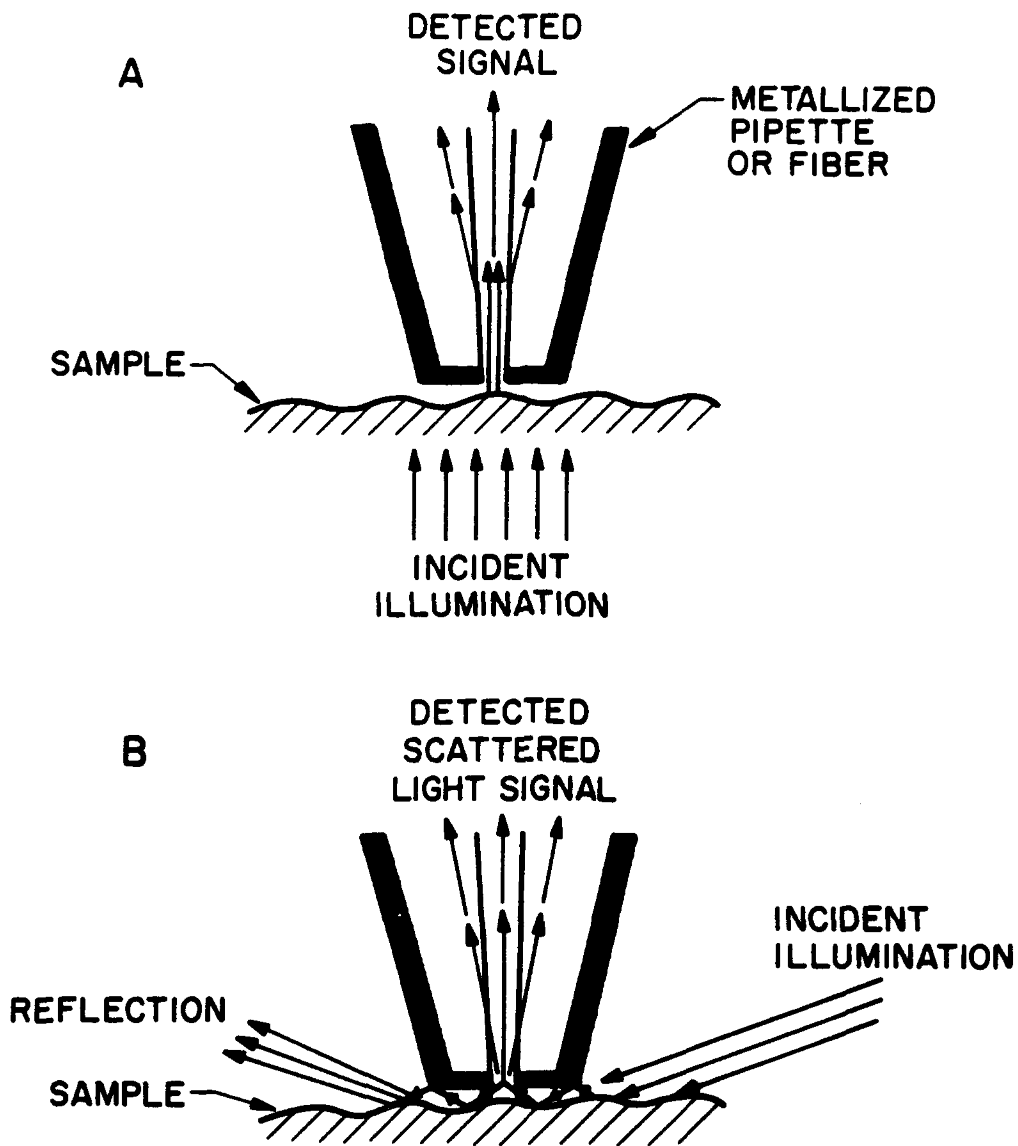

Figure 4: Schematic diagrams of different modes of near-field scanning optical imaging: those used presently.
A. Collection mode (or emissive mode for self-luminous object).
B. Angle illuminated reflection mode. Illumination comes into the sample at an angle. This mode can result in directional "shadowing" of the image.

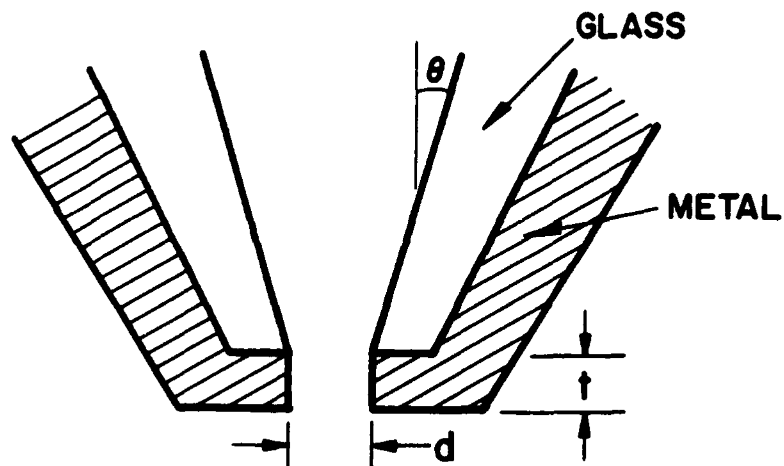

Figure 5: Schematic diagram of the metal aperture formed at the end of a drawn glass pipette. Note that the hollow core in this figure can be replaced with any index of refraction material.

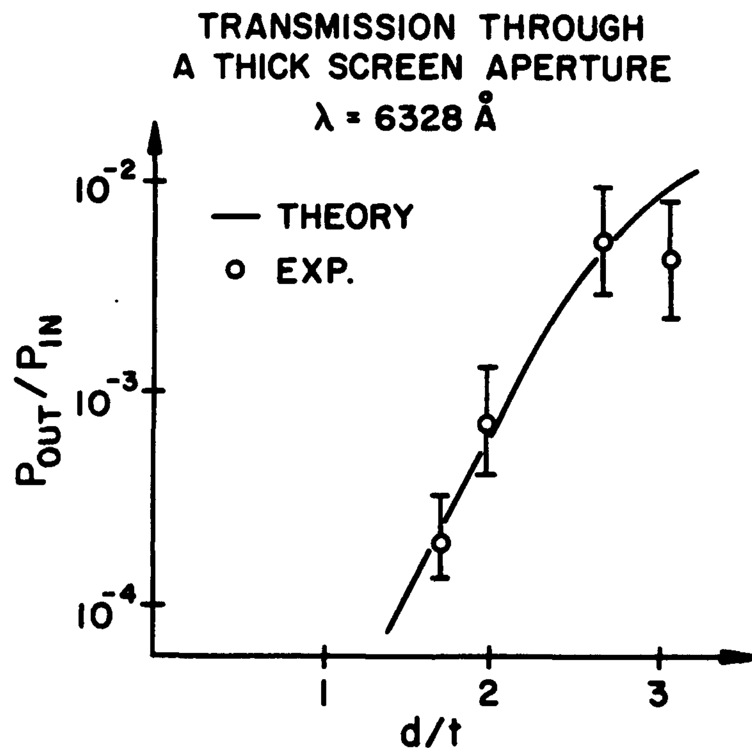

Figure 6: Optical transmission through a thick screen aperture at λ=6328Å. The calculations have been based on the method of Roberts (1987) assuming an aperture in a finite thickness, perfectly conducting screen. The measurements are based on light transmitted through an aluminum aperture of diameter d at the end of a drawn glass pipette (see Figure 5 for the pipette schematic). The power out, P_{out}, is that which is detected at the large end of the tube. Note that because of our experimental geometry, we do not necessarily expect the same values of transmission if we have light incident at the large end of the tube.

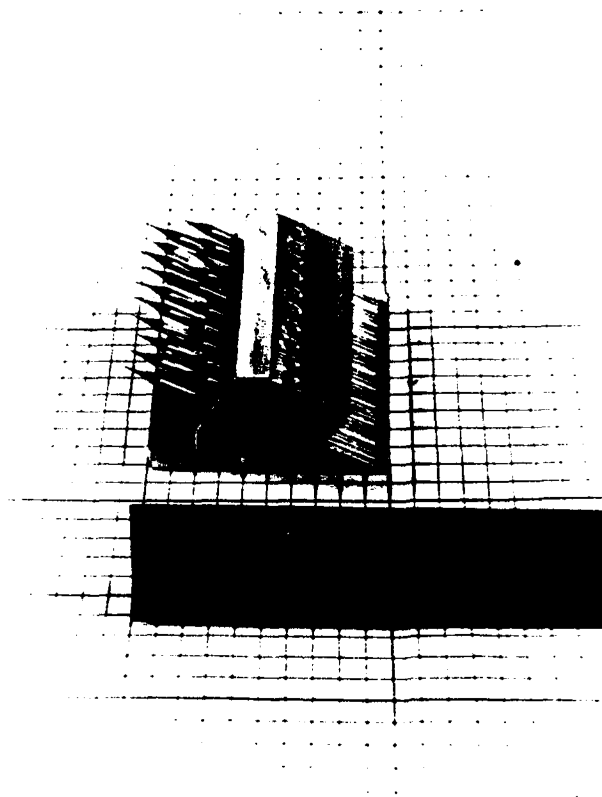

Figure 7: View of holder for 20 aluminum coated glass pipettes. This holder will be placed in an SEM for inspection of the coating, the final taper and aperture diameter.

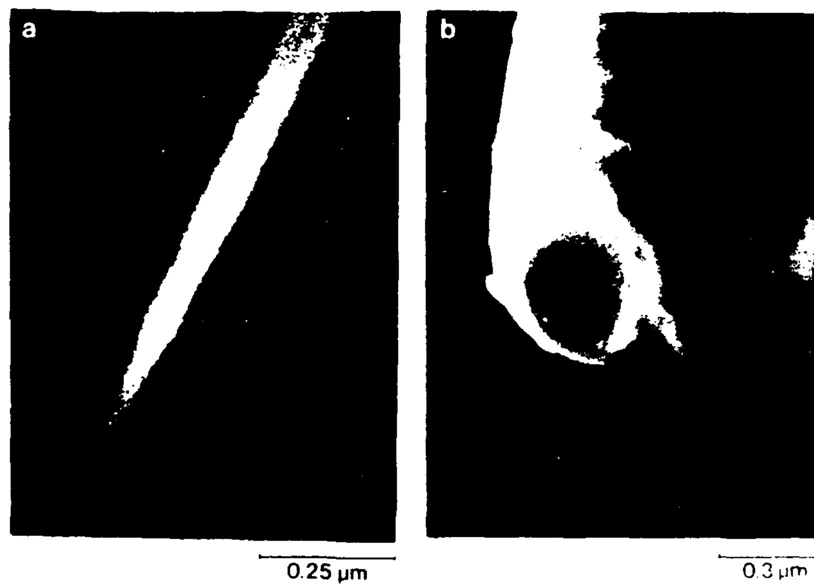

Figure 8: Scanning electron micrographs of uncoated borosilicate glass pipettes. The image at the right shows a 50nm diameter hole at the pipette tip whereas the image at the left shows that pipettes (although not hollow) with outer diameters as small as 25nm can be fabricated.

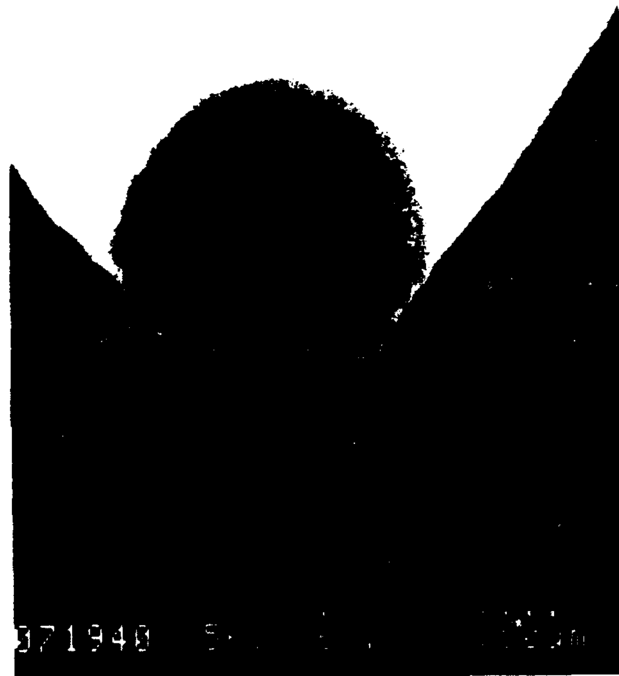

Figure 9: Above: Scanning electron micrographs (sideview and front view) of a chromium coated borosilicate glass pipette with an aperture diameter of 250nm. Below: Scanning electron micrograph of an aluminum coated borosilicate pipette with a 150nm diameter aperture.

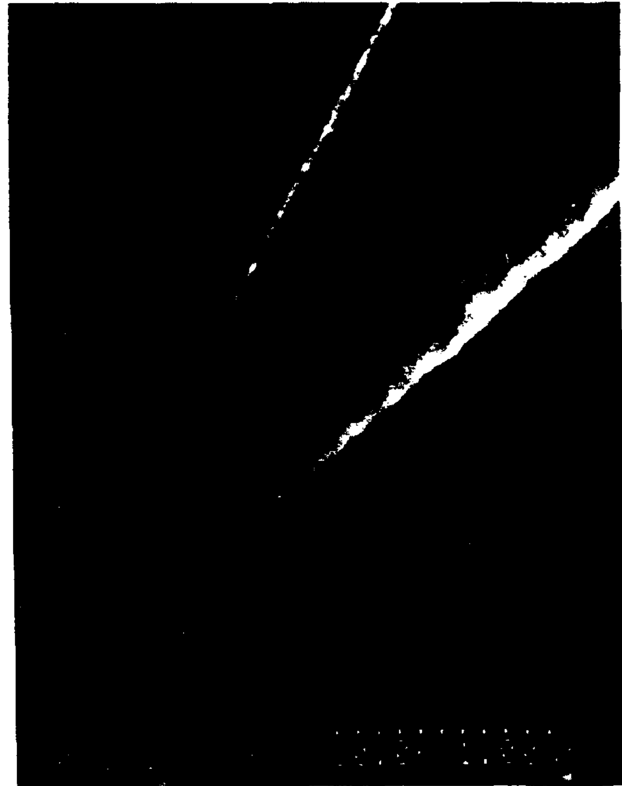

Figure 9b. Scanning electron micrographs of a pipette aperture fabricated from aluminosilicate glass. The advantage of using this rather than borosilicate glass is that because of the different melting point, the pipette end is slightly fire polished during the pulling process. This results in a slightly rounder and smoother end which allows for more uniform metal film growth.

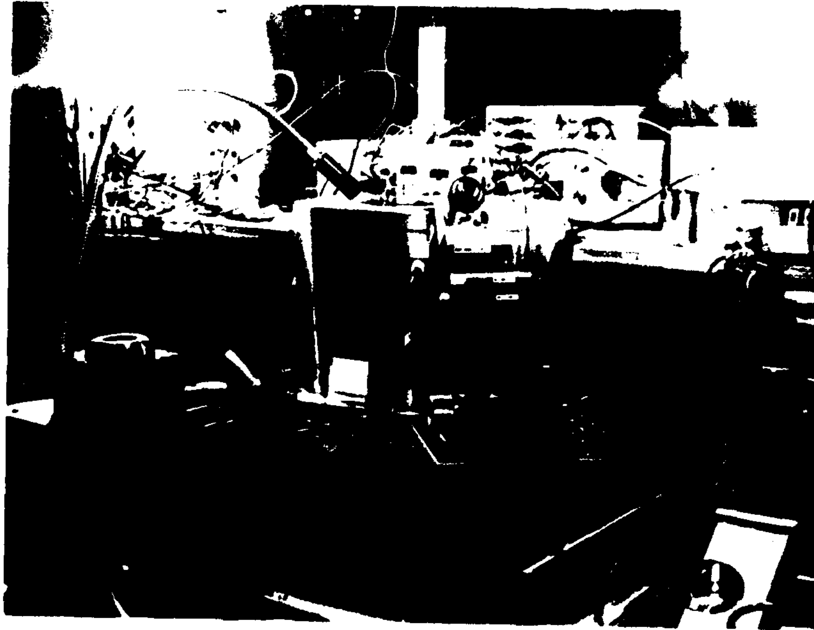

Figure 10: View of the existing near field microscope assembly on an optical table. A conventional microscope assembly is situated within the open port. The neck of a conventional white light fiber optic illuminator is shown to the left. This can be inserted to illuminate the sample from below or in reflection through a side port.

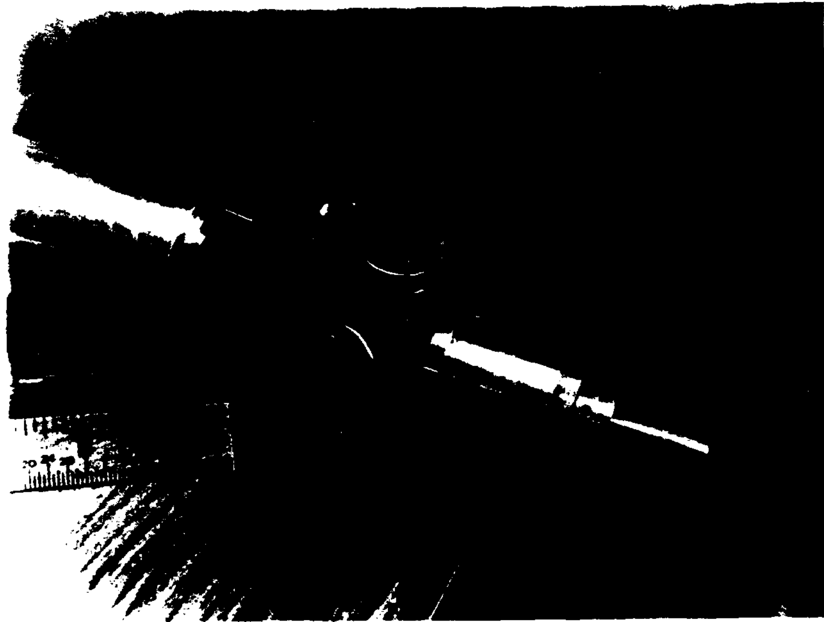

Figure 11: The pipette assembly of the microscope. The pipette is mounted in an aluminum holder attached to a piezoelectric tube, providing fine positioning in the z direction (perpendicular to the sample). In addition, a preamp for capacitance feedback is installed close to the probe for reduced electrical noise.

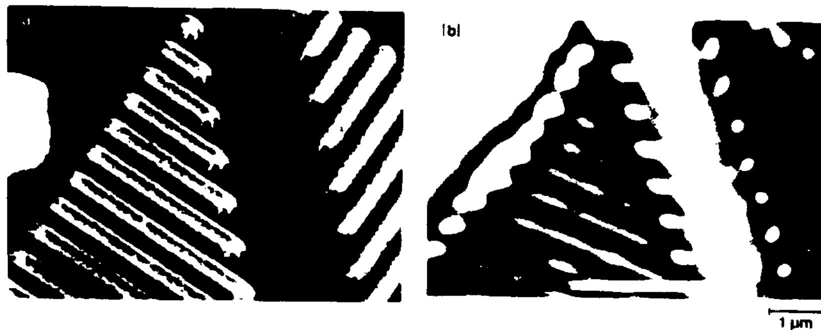

Figure 12: A. SEM micrograph of 250nm wide aluminum bars (bars appear bright).
B. Optical near-field transmission image of the bars (bars appear dark). Notice the transmission peaks near the ends of the bars. These peaks have been qualitatively explained by calculations done by Marx and Teague at the National Institute of Standards and Technology (1987).

Figure 13: Effect of aperture size on resolution. Near-field transmission images of a 250nm wide aluminum bar grating (bars appear dark). Image "a" taken with a 600nm ID pipette and image "b" a 150nm ID pipette. Note the higher resolution with the smaller ID pipette.

Figure 14: Comparison of a conventional phase contrast image (A) and near field scanning optical image (B) of a thin section of human skeletal muscle. The cell nucleus appears dark in both images, but the near field image only reveals the details near the surface even though the image was obtained in transmission.

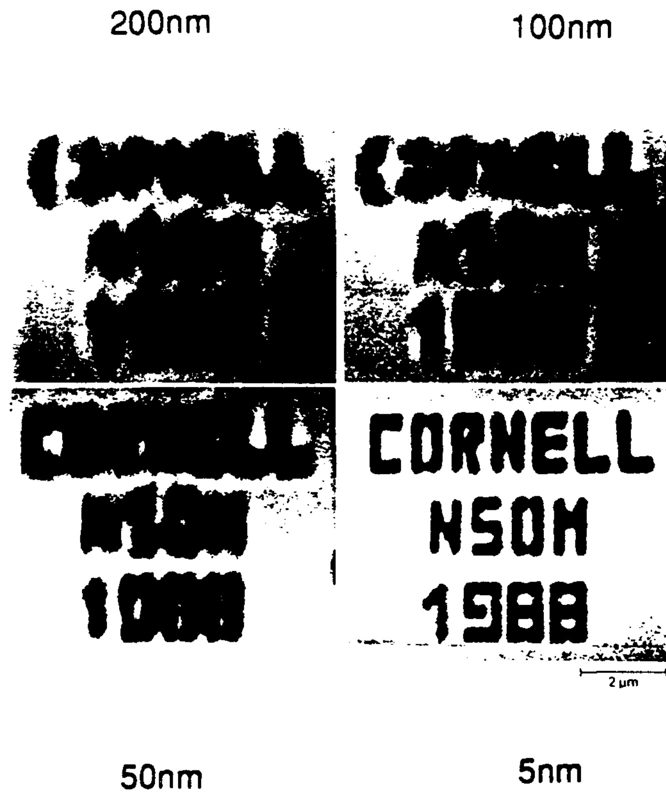

Figure 15: Effect of pipette to sample separation on resolution of non-periodic aluminum letters on a Si_3N_4 membrane. Images were taken in transmission using broadband arc lamp illumination with a 450nm cut-off filter. Distance of the pipette to sample is shown above. Note that the gap in the "O" is 50nm wide and becomes distinctly visible in the lower right image (i.e., the "near field" image).

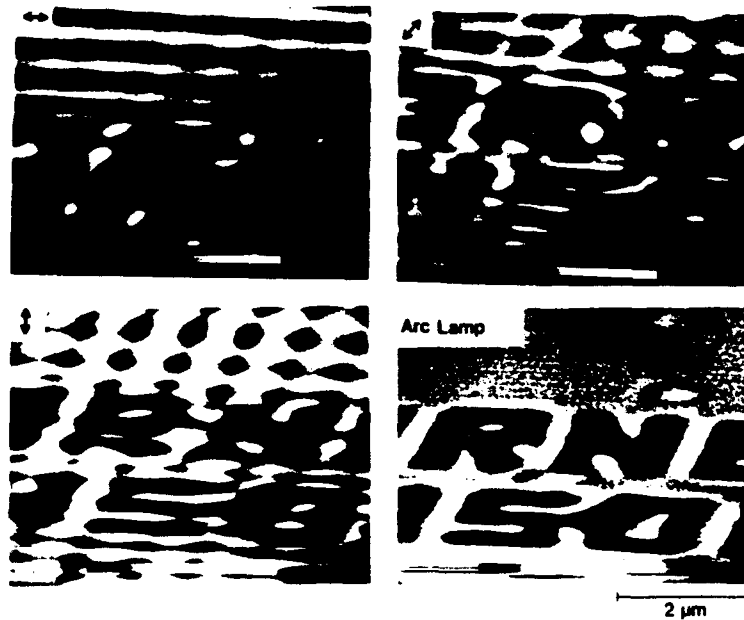

Figure 16: Effect of illumination on near-field transmission images of 25nmÅ thick aluminum structures on a Si_3N_4 membrane. Shown above are the images obtained using three different polarizations of a HeNe laser and broadband arc lamp illumination with a 450nm cut-off filter (only light with λ>450nm is passed).

unpolarized

1μ

Figure 17:
Effects of different polarization of the illumination on near-field images of 100nm aluminum dots on a bulk silicon substrate using coherent HeNe laser illumination. The lower right corner of the image corresponds to a part of the silicon wafer where there is no pattern. The polarization directions are indicated.

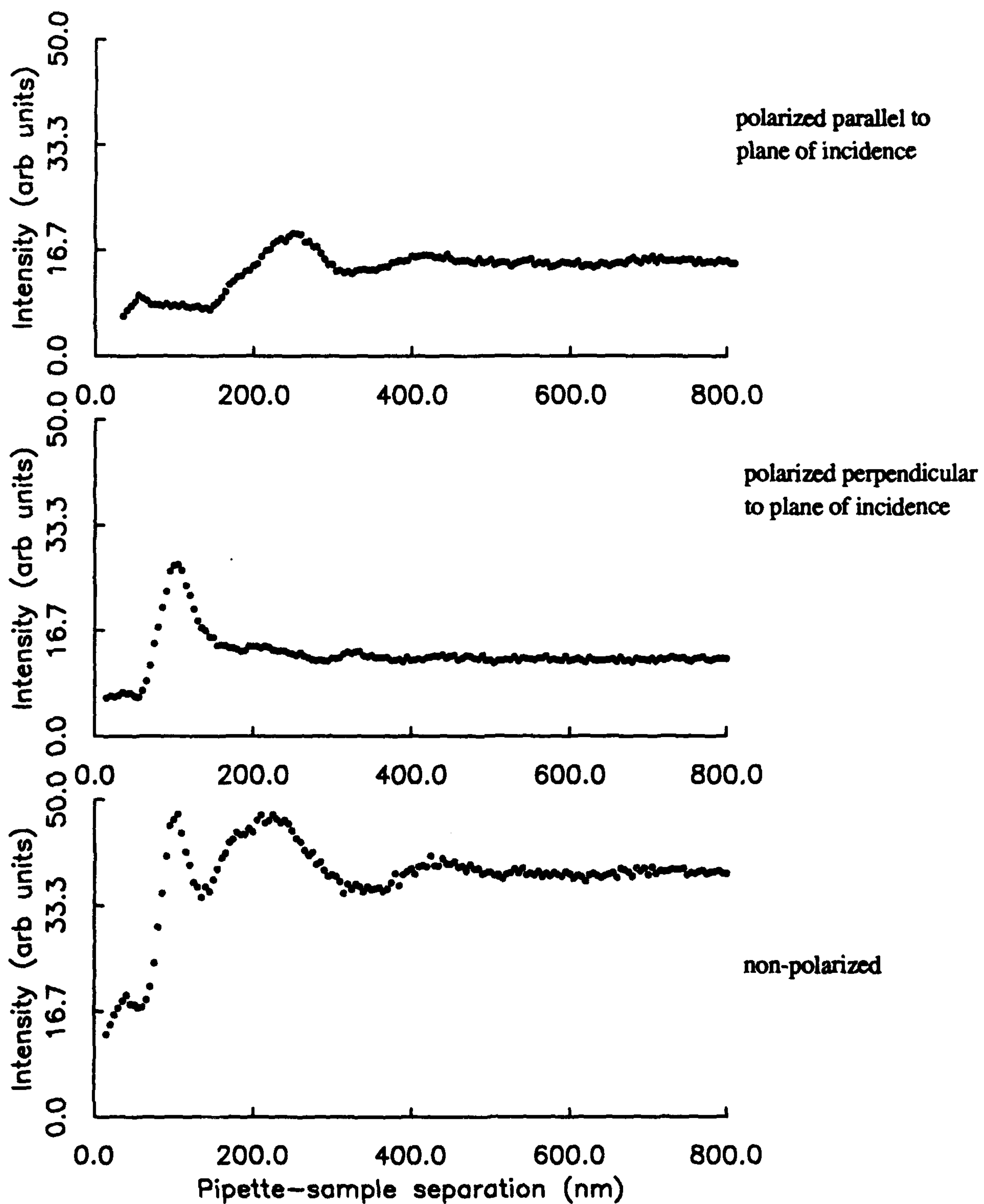

Figure 17b. Intensity collected through a 125nm diameter pipette aperture as a function of aperture distance from the surface of a thin aluminum film. The sample is illuminated with broad band light (λ>450nm) as shown in Figure 4b with a illumination angle (with respect to the surface) of 35°.

Figure 18: Near-field optical image of an array of 600Å diameter aluminum posts, 250Å thick on a 1400Å thick Si_3N_4 membrane. The upper image has been smoothed using a simple processing program developed for our IBM AT computer acquisition system.

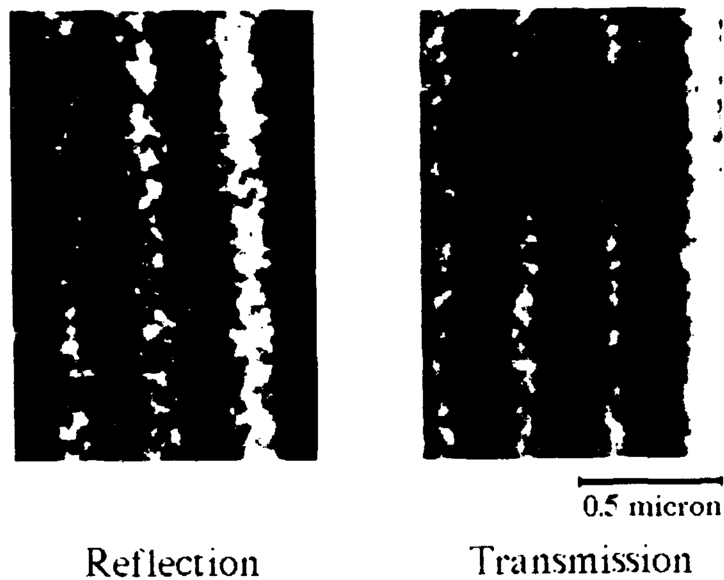

Figure 19: Near-field optical images of aluminum bars on a transparent Si_3N_4 membrane demonstrating both transmission and reflection mode high resolution capabilities. Images were taken with a broadband arc illumination, a 450nm cut-off filter and a 140nm ID pipette scanned 15nm from the surface. The aluminum bars (appearing dark in transmission and bright in reflection) are 76nm wide with 220nm spaces between them.

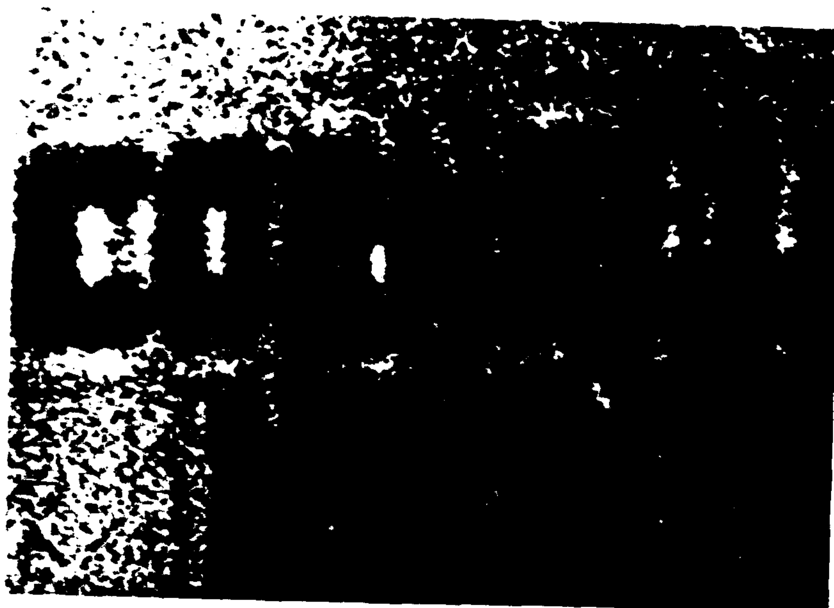

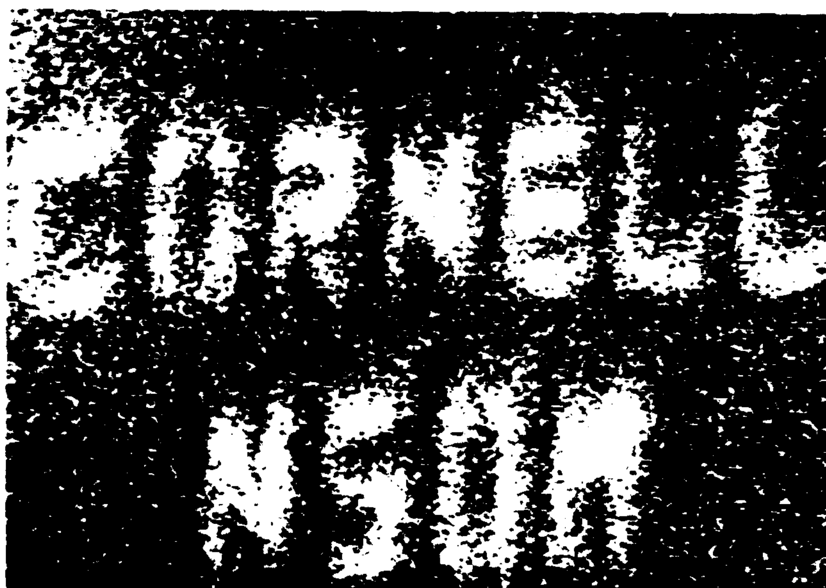

Figure 20: Scanning optical pipette transmission (upper) and reflection (lower) images of non-periodic aluminum letters on a transparent Si_3N_4 membrane. Images were taken with broadband arc lamp illumination and a 150nm ID pipette 200nm from the surface. Horizontal field of view is 15μm.

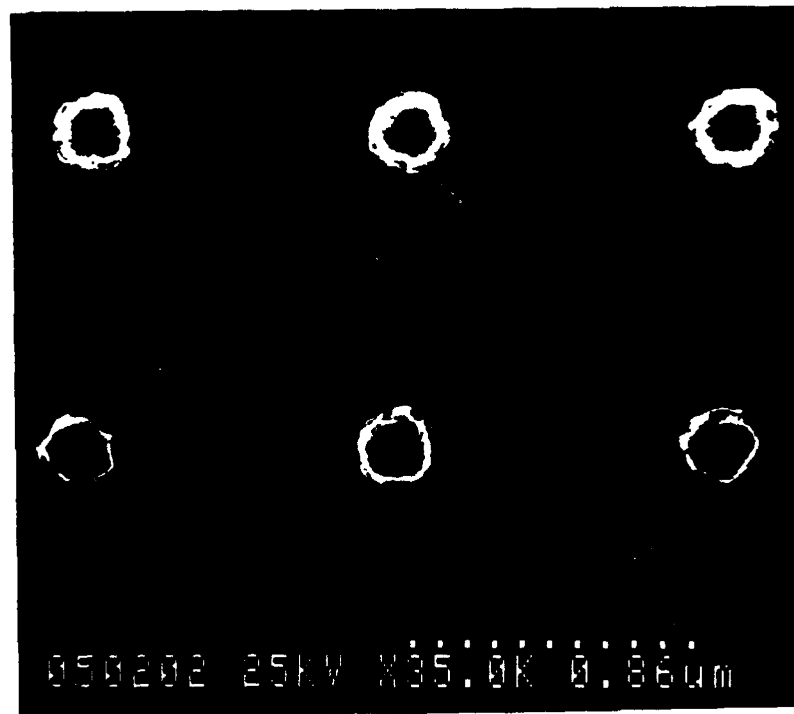

Figure 21A: Upper image: Optical near-field reflection image of 100nm thick aluminum dots on bulk silicon substrate. The sample was fabricated using a bi-layer resist and lift-off. The image was taken under broadband arc lamp illumination with a 160nm ID pipette scanned 10nm from the surface.
Lower image: SEM micrograph of the same sample at the same magnification as above. Notice the faint low-contrast shading around the dots in the SEM photo. This is most likely due to unremoved resist left on the sample after lift-off. In the near field optical image these differences in surface material characteristics are imaged with very high contrast.

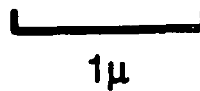

Figure 21B: Optical scanning pipette images: Far-field (upper, pipette ~800nm away) and intermediate field (lower, pipette ~60nm away) reflection mode images of aluminum dots on a bulk silicon substrate. Broadband arc illumination was used with a 450nm cut-off filter.

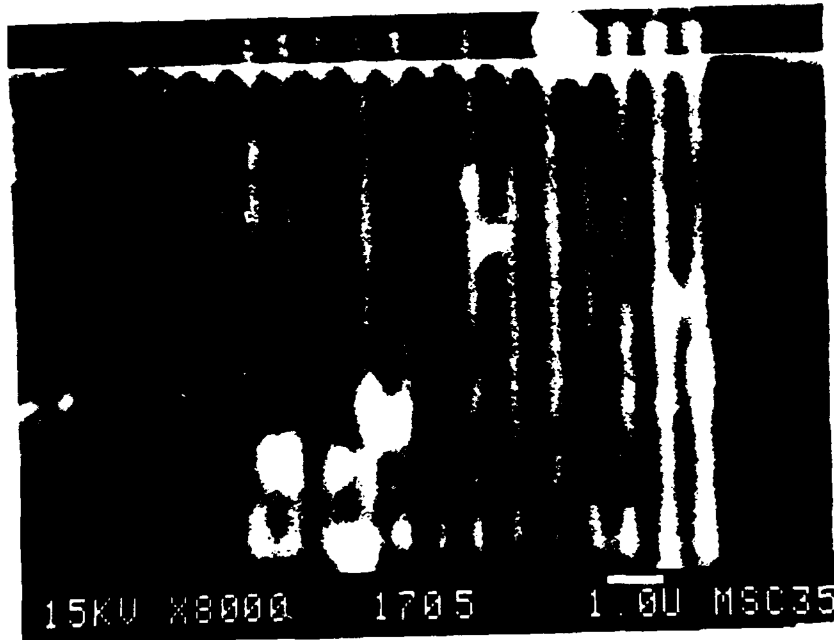

Figure 22: SEM micrograph of a grating pattern exposed in a 600Å thick Shipley 1400 resist on a silicon wafer. The pattern was exposed by contact printing of a metallized Si_3N_4 membrane mask of Hg-Xe lamp with 450nm cut off filter and demonstrates replication of 0.12μ lines on .25μ pitch.

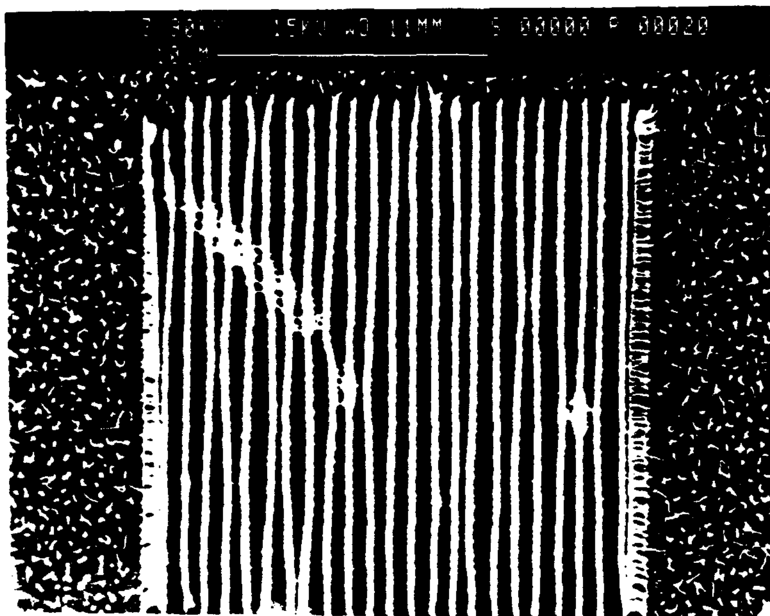

(A)

(B)

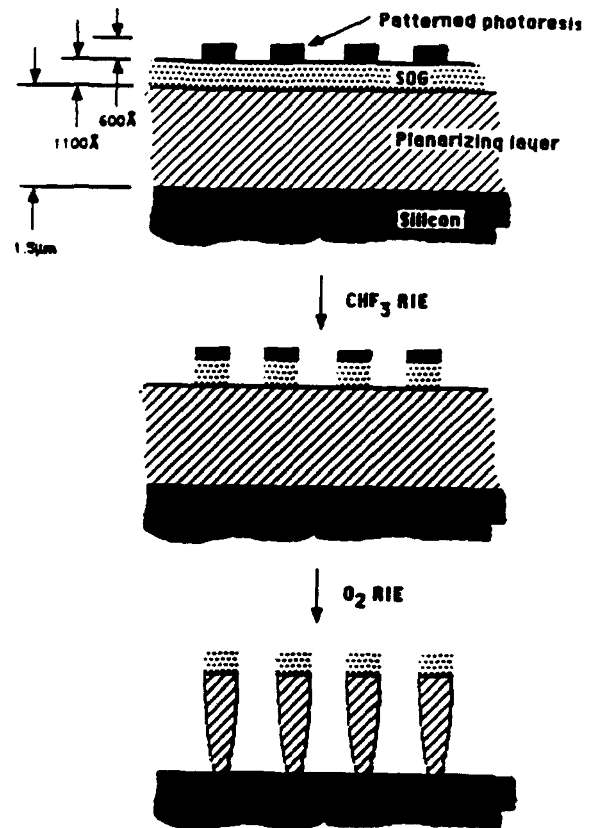

Figure 23: Examples of a pattern exposed in the near field using a tri level resist process. The three levels consist of a 600Å imaging layer of Shipley 1400 resist, an intermediate layer of spin-on-glass (Futurex ICI-200) and a 1.5µ thick polyester polymer planarzation layer (Futurex 150d). The process is indicated schematically at the right. A. SEM micrograph of a planar view of the RIE etched pattern showing 0.12µ lines and 0.2µ spaces.
B. SEM micrograph of higher magnification cross sectional view of pattern similar to that in A.

A

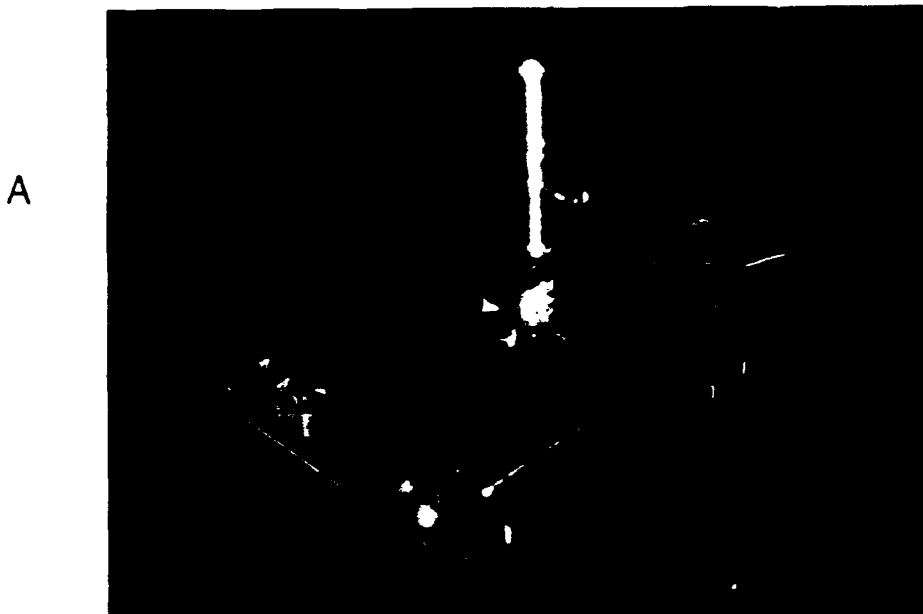

B

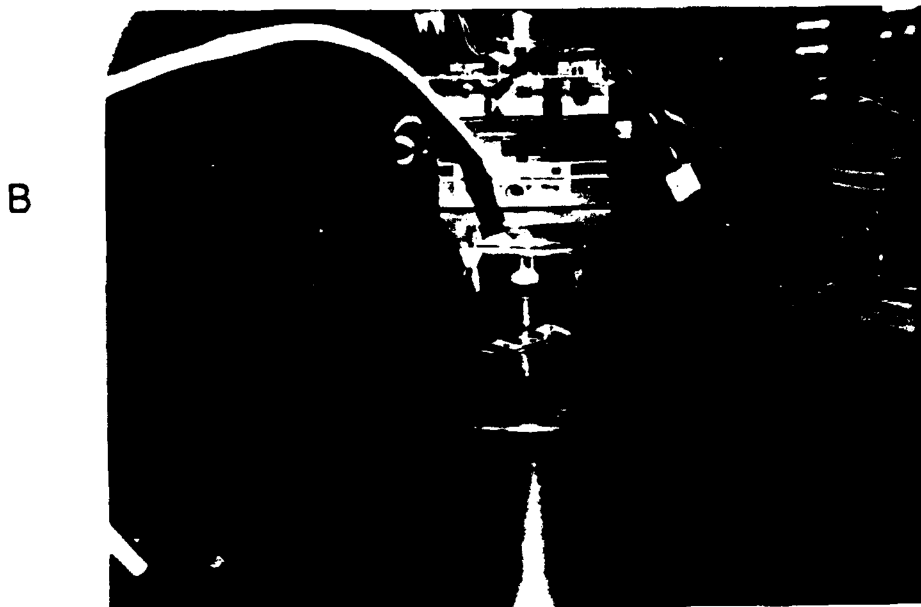

Figure 24: A. View of an exposed laser (GRIN-SCH-SQW) from McDonnell-Douglas underneath the pipette collector (which is mounted on a piezo tube stack).
B. More distant view of (A) showing the assembly within the microscope housing. A fiber optic illuminator lights the inside from the viewing port.

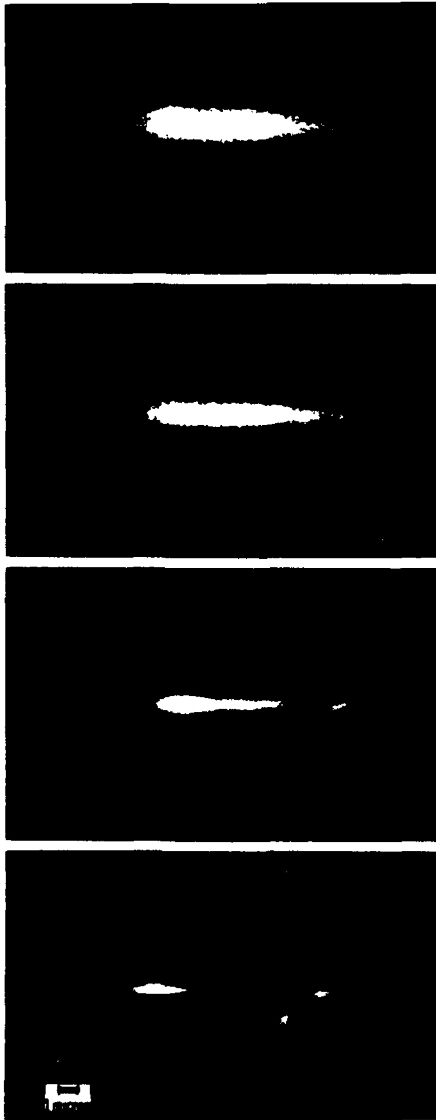

Figure 25:
Imaging of the modal field pattern of an AlGaAs GRIN-SCH-SQW diode laser supplied by Dr. Chet Balestra of McDonnell-Douglas Electronic Systems. The laser emission wavelength λ=860nm, and the pipette aperture used for imaging had a diameter of about $\lambda/6$. The sequence of images represents pipette-laser facet separations of, from top to bottom, $4\lambda/3$, $2\lambda/3$, $\lambda/3$ and $\lambda/100$. The resolution dramatically improves as the pipette approaches the laser facet. Conventional imaging methods are diffraction limited to resolution of roughly $\lambda/2$, and would indicate a pattern similar to the image at $2\lambda/3$ from the laser facet. Clearly there is increasing lateral structure and detail revealed in the high resolution near-field images. This particular laser displayed a so-called "rabbit ear" pattern, probably due to fabrication induced material strain. There may be evidence of dark line defects (DLDs) (Waters and Bertaska, 1988) at 45° to the horizontal in the vicinity of the two high intensity lobes. The uniform vertical lines on the left of the images are due to electrical interference and are not sample features.

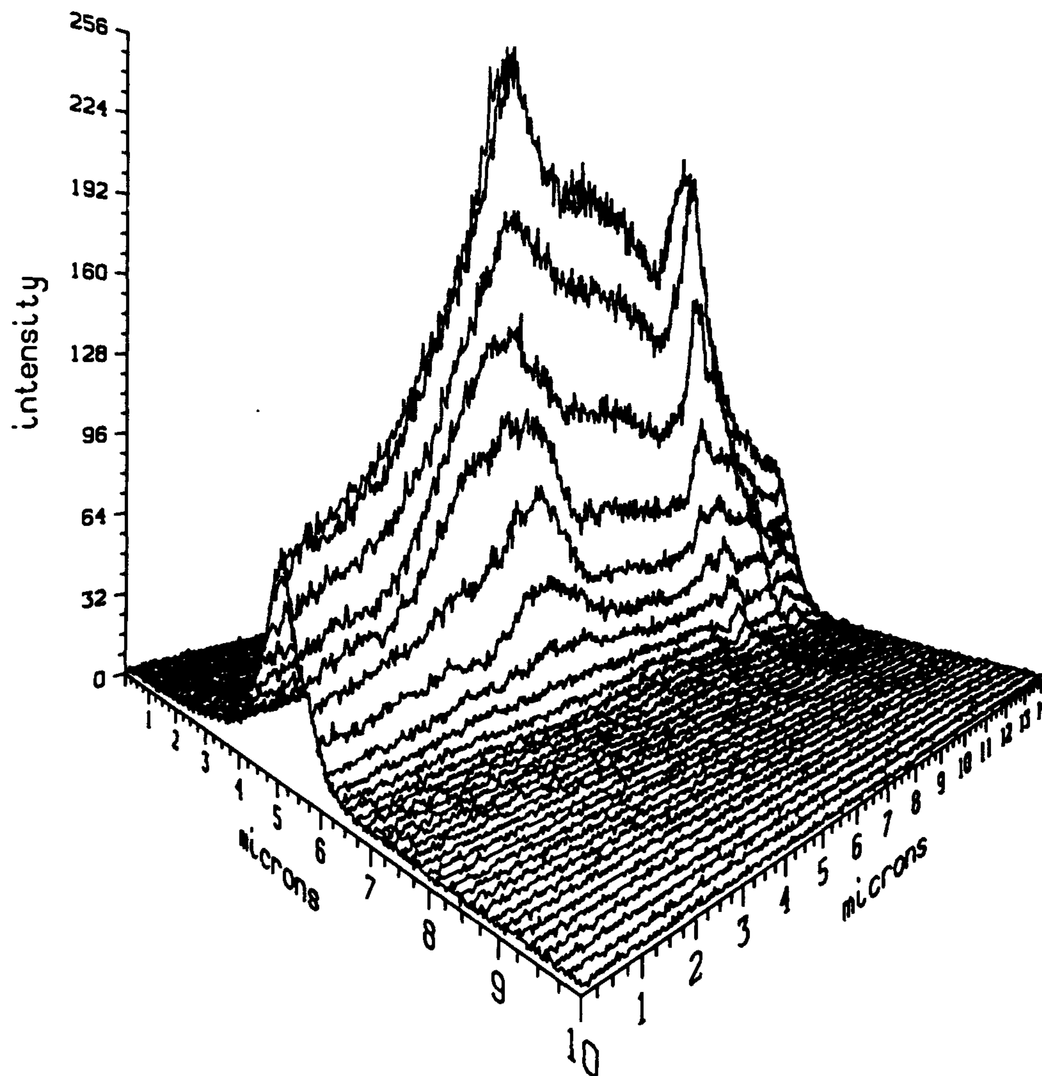

Figure 26: Series of intensity line scans corresponding to the near-field image at $\lambda/100$ distance from the laser facet (lower image in Figure 25). These scans are viewed from the bottom of the image. Note the intensity dips due to the dark line defects.

1μ

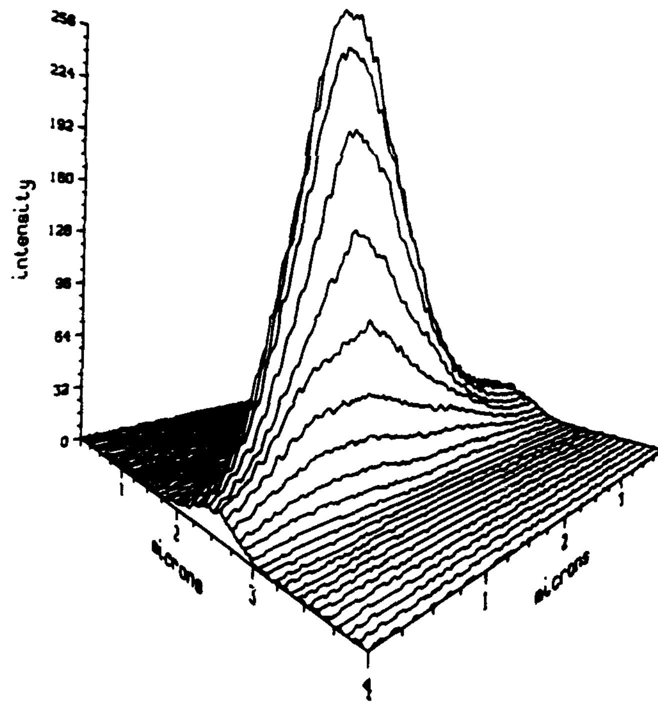

Figure 27: Top: Image of the model field pattern of a good Y rib AlGaAs GRIN-SCH-SQW diode laser from McDonnell-Douglas Electronic Systems. The laser emission wavelength λ=860nm and the pipette aperture was at λ/100 from the laser facet.
Bottom: Series of intensity line scans corresponding to the near field image shown above. The pipette aperture was 100nm in diameter.

III. APPENDICES

A. INVITED TALKS PRESENTING RESEARCH SUPPORTED UNDER CONTRACT AFOSR 87-0381

B. PAPERS PUBLISHED FROM 9/1/87 - 8/31/90 UNDER THIS CONTRACT

C. INVITED MANUSCRIPTS IN PREPARATION RELATING TO PRESENT CONTRACT RESEARCH

D. STUDENTS PERFORMING RESEARCH ON NEAR FIELD IMAGING AND LITHOGRAPHY

APPENDIX A

INVITED LECTURES - DISCUSSING RESEARCH PERFORMED UNDER PRESENT CONTRACT PERIOD: September 1, 1987 - August 31, 1990

1. September 1987. Osaka University, Dept. of Applied Physics, Osaka, Japan. "Near Field Microscopy and Lithography"

2. September 1987. 45th Annual Meeting, Electron Microscopy Society of America, Baltimore, Maryland. "Scanned Image Microscopies; An Overview"

3. November 1987. IBM Thomas J. Watson Research Center, Yorktown Heights, New York. Manufacturing Sciences Seminar. "Near Field Scanning Optical Microscopy"

4. January 1988. SPIE Meeting, Optoelectronics and Laser Applications in Science and Engineering, Los Angeles, CA. "Scanning Near Field Optical Microscopy"

5. March 1988. APS Meeting, New Orleans, Louisiana. "Near Field Optical Imaging"

6. June 1988. Shell Development Corporation, Westhollow Research Center, Houston, Texas. "Optical Methods for Structure Determination"

7. June 1988. InterMicro '88, Chicago, Illinois. "Near Field Optical Imaging"

8. August 1988. 46th Annual Meeting EMSA, Milwaukee, Wisconsin. "Near Field Optical Imaging"

9. September 1988. American Society for Metals, World Materials Congress, Chicago, Illinois. "Near Field Scanning Optical Microscopy"

10. October 1988. IMEKO XI, The 11th Congress of the International Measurement Confederation, Houston, Texas. "Near Field Optical Imaging"

11. November 1988. North Carolina State University, Physics Dept. Colloquium, Raleigh, North Carolina. "Near Field Optical Imaging"

12. December 1988. Bell Communications Research Laboratories, Red Bank, New Jersey. "Beyond the Diffraction Limit: Near Field Imaging"

13. December 1988. Fritz-Haber Institute, West Berlin, "Mikroskopie Ohne Lenses"

14. March 1989. Radiation Research Society Annual Meeting, Seattle, Washington. "Near Field Optical Imaging"

15. March 1989. University of Washington, Center for Bioengineering, Seattle, Washington. "Near Field Optical Imaging"

16. April 1989. New York State Dept. of Health Symposium on Frontiers in Biological Imaging, Albany, New York. "Near Field Optical Microscopy"

17. April 1989. Shell Development Corporation, Bellaire Research Center, Houston Texas. "Near Field Imaging"

18. June 1989. Gordon Research Conference on Three Dimensional Imaging, Plymouth, New Hampshire. "Near Field Imaging"

19. August 1989. 47th Annual Meeting EMSA, San Antonio, Texas. Presidential Symposium. "Three Hundred Years After Hooke and van Leuwenhoek: The Revolution in Optical Microscopy"

20. August 1989. Shell Development Company, Westhollow Research Center, Houston, Texas. "On the Potentials of Lenseless Microscopy for Inspection of Polymers and Rocks"

21. April 1990, Scanning '90, Washington, D.C.. "Potentials of Near Field Optical Microscopy"

22. April 1990, University of Washington, Dept. of Materials Science and Engineering, Seattle, Washington. "Near Field Imaging of Materials"

23. May 1990. SEM '90, Symposium on Scanned Tip Microscopies. "Prospects of Near Field Imaging"

24. August 1990. Shell Development Company, Westhollow Research Center, Microscopy Symposium. "Optical Imaging Without Lenses; Where Do We Go From Here?"

25. August 1990. 12th International Congress on Electron Microscopy, Seattle. "Near Field Optical Imaging"

APPENDIX B

PUBLICATIONS -- UNDER PRESENT CONTRACT PERIOD
September 1, 1987 - August 31, 1990

1. E. Betzig, M. Isaacson, A. Lewis and K. Lin, "Near Field Scanning Optical Microscopy" Proc. 45th Ann. EMSA Meeting, Baltimore, (San Francisco Press, 1987) 184-187.

2. A. Lewis, E. Betzig, A. Harootunian, M. Isaacson and E. Kratschmer, "Near Field Imaging of Fluourescence" in Spectroscopic Membrane Probes, Vol. II, ed. L.M. Loew (CRC Press, 1987) Chapter 12.

3. A. Lewis, M. Isaacson, E. Betzig and A. Harootunian, "The Near Field Optical Microscope", McGraw Hill Yearbook of Science and Technology (1987) 327-329.

4. E. Betzig, M. Isaacson and A. Lewis, "Collection Mode Near Field Scanning Optical Microscopy" Appl. Phys. Lett. 51, 2088 (1987).

5. M. Isaacson, "Near Field Scanning Optical Microscopy (NSOM)", Bull Am. Phy. Soc. 33(3), 414 (1988).

6. E. Betzig, M. Isaacson, H. Barshatzky, A. Lewis and K. Lin, "Superresolution Imaging with NSOM", Ultramicroscopy 25, 155 (1988)

7. E. Betzig, M. Isaacson, H. Barshatzky, K. Lin and A. Lewis, "Near Field Scanning Optical Microscopy", Proc. SPIE, Vol. 987 (1988) p. 91-99.

8. M. Isaacson, E. Betzig, H. Barshatzky and A. Lewis, "Near Field Imaging" Proc. 11th Congress IMEKO (1988).

9. M. Isaacson, E. Betzig, H. Barshatzky, K. Lin and A. Lewis, "Near Field Imaging" Microbeam Analysis 88 (D. Newbury, ed.) (1988) 417-418.

10. E. Betzig, M. Isaacson, H. Barshatzky, K. Lin and A. Lewis, "Progress in Near Field Scanning Optical Microscopy" Proc. 46th Ann. EMSA Meeting, San Antonio (San Francisco Press, 1989) 436-437.

11. M. Isaacson, "Three Hundred Years After Hooke and van Leuwenhoek: The Revolution in Optical Microscopy". Proc. 46th Ann. EMSA Meeting, San Antonio (San Francisco Press, 1989) 4-5.

APPENDIX C

INVITED MANUSCRIPTS IN PREPARATION RELATING TO PRESENT CONTRACT RESEARCH

1. M. Isaacson, H. Barshatzky and J. Cline, "Progress in Near Field Scanning Optical Microscopy", SEM 90, (ed. O. Johari; SEM, Inc., AMF O'Hare, Illinois) 1990.

2. M. Isaacson, "Scanned Tip Microscopies" Chapter in "Microscopy for the Life Sciences" (ed. F. Gillot; Univ. of Illinois Press) 1991.

3. M. Isaacson, et al., "Near Field Optical Imaging" Chapter in Advances in Physics (ed. S. Doniach, Taylor and Francis, Ltd., London) 1991.

4. M. Isaacson, et al., "Optical Imaging Without Lenses" in (ed. B. Jacobi, Plenum Press) 1991.

5. M. Isaacson, et al., "Near Field Optical Imaging Methods", AIP Workshop on Scanned Probe Microscopies (ed. K. Wickramasinghe and A. MacDonald) 1991.

APPENDIX D

STUDENTS PERFORMING RESEARCH UNDER PRESENT CONTRACT PERIOD: SEPTEMBER 1, 1987-AUGUST 31, 1990

Postdoctoral

Name	Present Location
Ernst Kratschmer (1986-87)	IBM General Technology Division, East Fishkill, NY

Ph.D.

Name	Present Location
A. Harootunian (1984-87)	Hughes Medical Research Center La Jolla, CA
E. Betzig (1984-88)	AT&T Bell Laboratories Murray Hill, NJ
J. Cline (1988 - present)	Cornell, School of Applied & Engineering Physics
H. Barshatzky (1985 - present)	Cornell, School of Applied & Engineering Physics

M.Eng.

Name	Present Location
I. Walton (1987 - 1988)	National Semiconductor, Santa Clara, California
R. Chen (1989 - 1990)	Digital Equipment Corporation
S. Boedecker (1990 - present)	Cornell, School of Applied & Engineering Physics
H. Chen (1990 - present)	Cornell, Department of Materials Science and Engineering

B.S.

Name	Present Location
M. Park (1987)	Cornell, School of Applied & Engineering Physics
M. Tornai (1988)	UCLA, Dept. Medical Physics, Los Angeles, California